

Article

Laser-Irradiated Chlorpromazine as a Potent Anti-Biofilm Agent for Coating of Biomedical Devices

Simona Nistorescu ^{1,2}, Gratiela Gradisteanu Pircalabioru ^{2,3,*}, Ana-Maria Udrea ^{1,2},
Ágota Simon ^{1,5}, Mihail Lucian Pascu ^{1,4,5} and Mariana-Carmen Chifiriuc ^{2,3,4}

¹ National Institute for Laser, Plasma and Radiation Physics, 077125 Magurele, Romania; simona.stroescu@inflpr.ro (S.N.); ana.udrea@inflpr.ro (A.-M.U.); agota.simon@inflpr.ro (Á.S.); mihai.pascu@inflpr.ro (M.L.P.)

² Faculty of Biology, University of Bucharest, 050095 Bucharest, Romania; carmen.chifiriuc@bio.unibuc.ro

³ Research Institute of the University of Bucharest (ICUB), University of Bucharest, 050095 Bucharest, Romania

⁴ Academy of Romanian Scientists, 050045 Bucharest, Romania

⁵ Faculty of Physics, University of Bucharest, 077125 Magurele, Romania

* Correspondence: gratiela87@gmail.com

Received: 23 October 2020; Accepted: 11 December 2020; Published: 16 December 2020



Abstract: Nowadays, antibiotic resistance has become increasingly common, triggering a global health crisis, immediately needing alternative, including repurposed drugs with potent bactericidal effects. We demonstrated that chlorpromazine aqueous solutions exposed to laser radiation exhibited visible activity against various microorganisms. The aim of this study was to investigate the quantitative antimicrobial activity of chlorpromazine in non-irradiated and 4-h laser irradiated form. Also, we examined the effect of both solutions impregnated on a cotton patch, cannula, and urinary catheter against Gram-positive *Staphylococcus aureus* and Gram-negative *Pseudomonas aeruginosa* and *Escherichia coli*. In all experimental versions, the chlorpromazine antimicrobial activity was enhanced by laser exposure. Besides the experimental results, the *in silico* analyses using molecular docking proved that the improved antimicrobial activity of the irradiated compound was a result of the combined action of the photoproducts on the biological target (s). Our results show that laser radiation could alter the molecular structure of various drugs and their effects, proving to be a promising strategy to halt antibiotic resistance, by repurposing current medicines for new antimicrobial strategies, thereby decreasing the costs and time for the development of more efficient drugs.

Keywords: chlorpromazine; Nd:YAG laser; anti-biofilm

1. Introduction

Nowadays, antibiotic resistant bacteria are a global public issue related to extended illness and high mortality rates [1,2]. Moreover, bacteria can adhere to abiotic or biotic surfaces, forming microbial biofilms that are more resistant both to antibiotic treatments and to host immune effectors [3,4]. In contrast to their planktonic counterparts, biofilm embedded cells are usually heterogeneous, both in term of taxonomy and physiology, and also are found in close proximity to each other, being covered with a protective extracellular matrix secreted by themselves [5,6].

Currently, a worldwide challenge is represented by the “health care-associated infections” (HCAIs), which involve increased administration of antibiotics. The most common HCAIs are classified wound infections (24.3%), urinary tract infections (23.2%), and lower respiratory infections (21.7%). For instance, the largest growth in infection rates was observed in diarrhea due to toxigenic *Clostridium difficile*, an ailment linked to antibiotic use. The increased prevalence of antibiotic-associated diarrhea is but one of the complications that can appear from increased antibiotic use; an even greater threat comes from increasing antimicrobial resistance of many nosocomial pathogens [7].

Generally, HCAs refer to an infection developed by a patient during or after hospital discharge [8]. Medical devices, like catheters, can be contaminated with microorganisms, so that they are the main culprits responsible for HCAs. Statistics show that 7–10% of patients get HCAs in developed versus developing countries [9]. The incidence of HCAs was reported by the World Health Organization to be about 4,544,100 episodes annually in Europe and 1.7 million in the USA [10].

Medical devices can be contaminated, mainly, by *Staphylococcus aureus* (*S. aureus*), *Pseudomonas aeruginosa* (*P. aeruginosa*), or *Escherichia coli* (*E. coli*) strains [11,12]. These microorganisms normally found on patients' skin, may be transferred from patient to patient or from patient to healthcare personnel. In addition, medical devices associated biofilm infections, contribute to an important extent to the burden of HCAs (e.g., urinary infections account for 33% of HCAs, 80% of these being associated with urinary an catheter [13,14].

Moreover, multiple drug resistant (MDR) bacteria, such as methicillin-resistant *S. aureus* (MRSA), which is the most prevalent MDR bacterium that has passed from the hospital environment into the community, vancomycin-resistant enterococci, and carbapenem-resistant *Acinetobacter baumannii*, as well as the emergence of novel resistance mechanisms worsen the fate of HCAI patients [15–17].

The researchers are looking for alternative strategies (probiotics, bacteriophages, antimicrobial peptides, bacteriocins) to fight these superbugs [18]. Phenothiazines are compounds mainly used to treat psychotic disorders and their primary antipsychotic action seems to be based on suppression of dopamine by blocking the dopaminergic receptors. Some derivatives, such as chlorpromazine (CPZ), thioridazine (TZ) and trifluoperazine (TPZ) were shown to have anticancer, antibacterial and antiviral activity. When the drug is administered to people that do not present psychosis, which means that the dopamine receptors are not blocked, phenothiazines may harbor other biological properties that worth further investigations [19–21].

In recent years, laser irradiation of non-antibiotics (such as phenothiazine derivatives) and antibiotics led to the photodegradation of the parental compounds into photoproducts with possible antimicrobial effect [21–23]. CPZ and TZ can cause photosensitivity, many patients expressing sunburn reaction and hyperpigmentation [24]. A high sensitivity to light was observed for substances with phenothiazine core structure, their aqueous solutions showing visible colour when exposed to laser radiation [22,23].

Irradiated CPZ is a mixture of CPZ and CPZ photoproducts generated in the solution after laser exposure, such as: chlorpromazine sulfoxide (CPZ-SO), promazine (PZ), promazine sulfoxide (PZ-SO), 2-hydroxy promazine (2-HO-PZ), 2-hydroxy promazine sulfoxide (2-HO-PZ-SO) and other three products [23].

Molecular docking is a technique generally used in rational drug-design to predict the interaction between a compound and a molecular structure [25,26]. We used it to predict the possible mechanism of the antimicrobial action of the irradiated and non-irradiated CPZ.

Our study was focused on testing CPZ, both unirradiated and laser irradiated, against various microorganisms of clinical importance, in planktonic and biofilm growth state. The antimicrobial and antibiofilm efficiency were determined by conventional methods: minimum inhibitory concentration (MIC) and minimum biofilm eradication concentration (MBEC). The stability of the irradiated as well as non-irradiated compounds was also evaluated by determining the MIC after four months from the preparation of the solutions. In addition, the ability of the antipsychotic drug to inhibit the bacterial adherence on medical devices was studied through the viable cells counts method, after submersion of the materials in CPZ solutions. We used a molecular docking approach to simulate the interaction between CPZ and its photoproducts with several *S. aureus* membrane proteins, in order to unveil the inhibitory mechanism responsible for CPZ activity.

2. Materials and Methods

2.1. Chemical Solutions and Laser Irradiation

Chlorpromazine (CPZ) (Sigma Aldrich, St. Louis, MO, USA) was dissolved in ultrapure water at 20 mg/mL concentration. The ultrapure de-ionized water was delivered via a sterile filter (TKA Smart2Pure UV) with 0.055 $\mu\text{S}/\text{cm}$ conductivity at 25 °C. Stock solutions of 2 mL were irradiated 4 h in a quartz cuvette with optical path length of 1 cm, using the fourth harmonic at 266 nm of the fundamental beam of a Nd:YAG pulsed laser (Surelite II, Continuum, Excel Technology, New York, NY, USA) at an average energy of 6.5 mJ. The pulse repetition rate was 10 pulses per second, and the pulse time width was 6 ns. The irradiation protocol is described in detail in Ref. [22].

The physicochemical characterization of solutions was made through UV-Vis-NIR absorption and Fourier-transform infrared (FTIR) spectra analyses in Refs [22,23]. The samples were qualitatively evaluated via thin layer chromatography and laser induced fluorescence in Refs [27,28].

2.2. pH Measurements

The pH measurements were made with a pH-meter (Lab 860 Schott Instruments), equipped with Blueline 16 pH electrode.

2.3. Microbial Strains

The antimicrobial activity of CPZ photoproducts was studied on standard and clinical isolates of Gram-positive bacteria *Staphylococcus aureus* ATCC 6538 (*S. aureus*), methicillin resistant *S. aureus* (MRSA1 and MRSA2), *Enterococcus faecalis* ATCC 29212 (*E. faecalis*) and Gram-negative bacteria *Pseudomonas aeruginosa* ATCC 27853 (*P. aeruginosa*), *P. aeruginosa* clinic1, and *P. aeruginosa* clinic2, *Escherichia coli* ATCC 8739 (*E. coli*), as well as a fungal strain, *Candida parapsilopsis* ATCC 22019 (*C. parapsilopsis*).

2.4. Determination of Minimum Inhibitory Concentration (MIC)

All strains were cultivated under the same conditions in plates with nutrient broth, at 37 °C for 18 h. The minimum inhibitory concentration (MIC) represents the lowest concentration of an antimicrobial drug that can inhibit bacterial growth and it was determined in Mueller Hinton broth medium, using the two-fold microdilution assay in 96 multi-well plates, following the ISO standard 20776-1, 2006 guidelines for antimicrobial susceptibility testing of non-fastidious organisms [29]. The stock solution was diluted down to 200 $\mu\text{g}/\text{mL}$. In a 96-well plate, 90 μL of nutrient broth was pipetted subsequently in all wells; 90 μL of test compound dilution was transferred into the first well, and serial dilutions were made until the last dilution; after words, 90 μL was discarded (the concentration started from 100 $\mu\text{g}/\text{mL}$ and reached 0.19 $\mu\text{g}/\text{mL}$ in the last well). For both, non-irradiated and irradiated CPZ solutions, the same steps have been followed. Finally, 10 μL of microbial suspension was added into each wall. Each sample of microbial suspension was prepared in a cell with 5 mL phosphate-buffered saline (PBS) over which a small amount of one microorganism culture with a sterile buffer was added. The microbial suspension was adjusted to 6 log CFU/mL, corresponding to a density of 0.5 McFarland. Every tested strain had a negative control (NC) and a positive control (PC) in the plate. MIC values were obtained after 18 h incubation at 37 °C, by reading the absorbance at 620 nm with a UV-Vis spectrophotometer.

2.5. Minimum Biofilm Eradication Concentration Assay (MBEC)

The evolution of microbial biofilms on inert substrate was studied in 96-well plates. The culture was grown in nutrient broth and in the presence of the same concentrations of non-irradiated/irradiated CPZ with the MIC assay (100–0.19 $\mu\text{g}/\text{mL}$); the incubation time was 18 h at 37 °C. In order to eliminate non-adherent cells, the culture medium was discarded, and wells were washed with PBS,

being subsequently fixed with 100% methanol for 15 min. Further, the microplates were emptied, and the biofilm was stained with 1% violet crystallized alkaline solution (200 $\mu\text{L}/\text{well}$) for 15 min. Additional washing steps were needed to clean-up the surplus. In the microplates, 200 $\mu\text{L}/\text{well}$ of 33% acetic acid was added, the lowest drug concentration required to eliminate a microbial biofilm (MBEC) being measured at 490 nm absorbance.

2.6. Immersion of Medical Devices

Urinary catheter (size 16 Fr, Shanghai Channelmed), cannula (Healfon) and standard unsoiled 100% cotton fabric DIN 53919/ISO 2267 (standard ISO 2267:1986), patch wfk Testgewebe) were tested in contact with the -irradiated and irradiated CPZ solution and the bacterial strains, using the protocol adapted from Leanne Fisher et al. [30]. Prior to the protocol, the cotton fabric underwent a cleaning procedure, consisting of 10 washing cycles in warm tap water, to eliminate contaminations. To verify the cleanliness of the fabric, the surface tension of the water used for washing was measured in each cycle with a Drop and Bubble Shape Tensiometer PAT-1 (SINTERFACE Technologies, Berlin, Germany), until the value of 71–72 mN/m was achieved, as shown in Simon et al. and Morán et al. [31,32]. Segments of 1 cm length were cut from a urinary catheter using a scalpel blade, then every piece was UV sterilized for 15 min on both sides. In the second step, all pieces were submersed for 1 h in 1 mL of non-irradiated/irradiated CPZ solution at a concentration of 1 mg/mL; during the impregnation, the samples volume doubled. Finally, the urinary catheter was washed in absolute ethanol and left to dry overnight in a current of air, at room temperature. These steps are shown in Figure 1. Using the same protocol, the cannula and the cotton patch were impregnated with CPZ solution. Experiments were performed in triplicate.

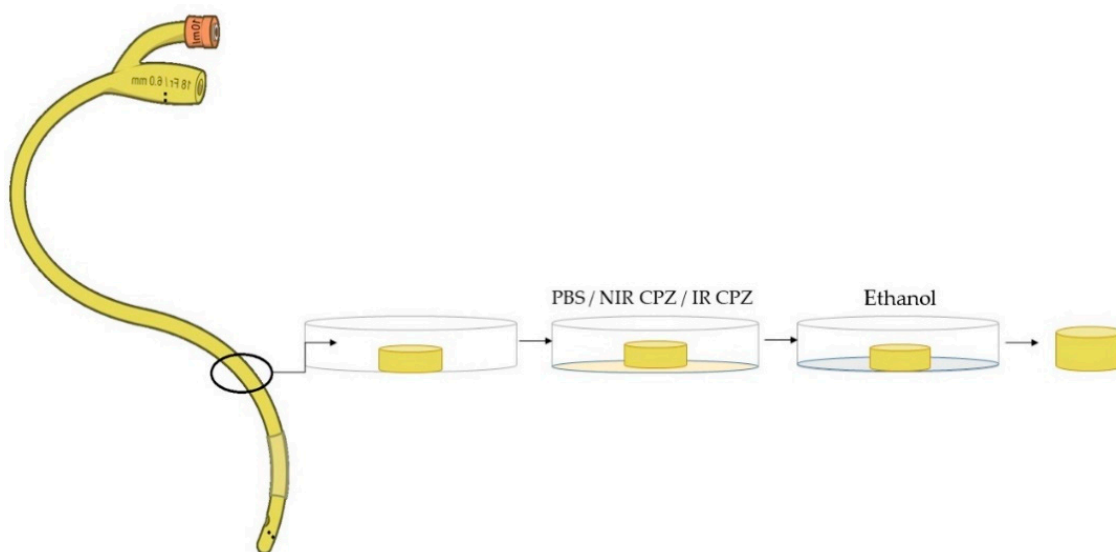


Figure 1. The protocol for the immersion of urinary catheter segments with non-irradiated/irradiated CPZ or PBS control. Legend: PBS = phosphate-buffered saline, NIR-CPZ = non-irradiated CPZ and IR-CPZ = irradiated CPZ.

2.7. Antibiofilm Assay

After successful impregnation of medical devices with CPZ solutions, the microbes were left 24 h in contact with tested materials. The bacterial adherence was analysed for four microbial strains including *E. coli*, *P. aeruginosa*, *S. aureus*, and *C. parapsilosis*. *S. aureus* and *E. coli* are among the main causes of postoperative infections, especially in surgical sutures where cotton is used to cover the wound [33]. The bacterial suspensions were prepared in minimum essential medium (MEM), corresponding to 10^6 CFU/mL. From each suspension, 1 mL/sample was aspirated and placed over the

3 types of aliquots: control, non-irradiated CPZ and irradiated CPZ. The plates with medical devices were left in the incubator for 18 h at 37 °C.

The bacterial adherence to the treated materials was determined through the viable cell counts method. After 18 h incubation, all medical material pieces were transferred in Eppendorf tubes, where 1 mL/tube containing sterile saline solution. The tubes were stirred for 1 min using a vortex. In 96 multi-well plates, a volume of 90 µL sterile saline solution was added together with 10 µL from each tube containing the materials.

Serial dilutions were performed up to 10^{-6} . Three replicate samples of 5 µL solution were pipetted from the serial dilutions at each concentration for determining the colony forming unit (CFU) values.

2.8. Computational Approach

To depict the inhibitory mechanism responsible for CPZ activity, we used a molecular docking approach to simulate the interaction between CPZ and its photoproducts and several membrane proteins from *S. aureus* involved in the interaction with antimicrobial substances.

We used: (i) five membrane proteins from *S. aureus*: enoyl-acyl carrier protein reductase enzyme (FabL), Protein Data Bank (PDB) code: 6TBB [34]; the bacterial cell-division protein (FtsA), PDB code: 3WQU [35]; Penicillin-Binding Protein 2a (PDB2a) from MRSA, PDB code: 5M18 [36]; Penicillin-Binding Protein 3 (PBP3) from MRSA, PDB code: 3VSL [37] and Penicillin-Binding Protein 4 PDB code: 5TWB [38], (ii) two membrane proteins from *P. aeruginosa*: PBP3, PDB code: 3OC2 [39] and Penicillin-Binding Protein 5 PBP5, PDB code: 4K91 [40], (iii) one *E. coli* protein, i.e., PBP3, PDB code: 4BJP [41].

Penicillin Binding Proteins (PBPs) are a class of proteins with high affinity for penicillin and β -lactam antibiotics, which catalyze the transpeptidation and transglycosylation steps of cell wall synthesis [42]. These proteins are divided in a low-molecular-weight (LMW) PBPs and 2 classes of high-molecular-weight (HMW) class A and class B. Class A PBPs catalyze transglycosylation and transpeptidation, class B PBPs have transpeptidase activity and LMW acts as d-d carboxypeptidase, being involved in cell wall maturation without being crucial in the biosynthesis of the peptidoglycan [43]. In our study we selected four class B PBPs: PBP2a and PBP3 from *S. aureus*, PBP3 from *E. coli* [44] and PBP3 from *P. aeruginosa* [45] as well as two LMW PBPs: PBP5 from *P. aeruginosa* [46] and PBP4 from *S. aureus* [44].

FtsA is a protein involved in cell division that assembles the Z ring of the cell, which allows the separation of daughter cells [35].

FabL is an essential enzyme in the biosynthesis of fatty acids and may represent a new target for the development of a new class of compounds active against *S. aureus* [34].

The 3D structure of proteins was taken from RCSB Protein Data Bank (Table 1) and was prepared for molecular docking studies by deleting water, adding hydrogen and merging the non-polar hydrogens also. Gasteiger partial charges were computed.

The compounds were modelled and geometrically optimized using Discovery Studio visualizer [BIOVIA, Dassault Systèmes, [47]. For molecular docking approach, we have used Autodock 4.2.6 software [48]. Grid-box was selected to contain only the active situs of proteins identified by specific amino acid (AA) residues (Table 1). Covalent grid parameters had an energy barrier height of 1000 and half-width of 5.0 Å [49].

Table 1. Proteins selected for molecular docking approach. PDB code of the protein, AA residues from the situs of interaction. In this table, we also present the grid box parameters introduced in Autodock 4.2.6 software to generate the grid box for each molecular docking model: grid points in dimension (x, y, z) and the coordinates of central grid point of the map.

Protein	PDB Code	AA Residues from Situs	Grid Points in Dimension	Coordinates of Central Grid Point of Map
<i>S. aureus</i>				
PBP3 MRSA	3VSL [37]	Active site: Ser392, Asn450, Ser448, Gln524, Thr603, Lys618, Gly620, Thr621, Glu623, Pro660 [37]	x 96 y 96 z 92	x 19.57 y -48.21 z 25.08
FtsA	3WQU [35]	Active site: Glu251, Lys254, His255 [35]	x 80 y 78 z 80	x 4.46 y 34.68 z -15.30
		Allosteric site: Ile314, Lys 316, Lys318, Asp320	x 86 y 80 z 92	x 12.81 y -24.85 z -63.08
PBP2a MRSA	5M18 [36]	Active site: Lys28, Lys86, Lys90, Lys148, Lys180, Lys181, Lys219, Met220, Tyr 223, Glu222, Glu268, Glu378, Lys382, Lys436, Tyr446, Gln502, Ser504, Asn505, Lys506, Asn507, Glu566, Glu602, Leu603, Lys604, Met605 Lys606, Gln607, Gly608, Glu609, Thr610, Gly611, Arg612 [36]	x 84 y 84 z 80	x 24.59 y -27.21 z -5.68
PBP4	5TW8 [38]	Active site: Ser75, Lys78, Ser139, Asn141, Lys259, Thr260 [38]	x 66 y 66 z 66	x 33.58 y -66.46 z 37.31
FabL	6TBB [34]	Active site: Ala96, Phe96, Ala97, Met99, Leu102, Tyr147, Gln155 Asn156, Tyr157, Met160, Pro192, Leu196, Ser197, Ala198, Phe204, Ile207 [34]	x 70 y 66 z 70	x -14.45 y -17.81 z -76.36
<i>E. coli</i>				
PBP3	4BJP [41]	Active site: Ser307, Lys310, Ser359, Asn361, Phe417, Gly418, Tyr419, Lys494, Thr495, Thr497, Lys499 Tyr514 [41]	x 68 y 68 z 68	x -6.55 y 22.76 z 13.37
<i>P. aeruginosa</i>				
PBP3	3OC2 [39]	Active site: Glu291; Ser294, Lys297, Ser349, Asn351, Tyr407, Tyr409, Lys484, Ser485, Thr487, Arg489, Tyr501, Tyr530, Phe531 [39]	x 66 y 66 z 66	x -0.93 y 1.95 z -17.89
PBP5	4K91 [40]	Active site: Ser41, Lys44, Ser101, Ser203 [40]	x 56 y 56 z 56	x 41.05 y -5.76 z 12.71

Table 1 presents the grid points in dimension and the cartesian coordinates of the central grid point of the map for each protein used in docking studies. The grid points spacing is 0.375 Å. Using the Lamarckian Genetic Algorithm search parameter, we have generated 100 runs for each ligand. This algorithm generates and optimizes a population of ligand positions using three operators: selection, crossover and mutation. In this study, we have used a hybrid model Lamarckian algorithm with software recommended parameters (150 individuals in the population; maximum of 2,500,000 energy evaluations; 27,000 maximum number of generations, 1 top individual that survive to next generation; the rate of crossover 0.8, a rate of gene mutation of 0.02 and a window size of 10). The Genetic Algorithm search parameter starts with a randomly generated population of individuals and generates new individuals using the previously mentioned operators. After each run, the population of individuals is replaced with the newly generated ones [48,50].

3. Results

3.1. Molecular Docking

A compound with low free binding energy presents a high biological activity; molecules with an energy of binding (kcal/mol) higher than -6 kcal/mol are defined as compounds with no biological activity on that target. We have used Autodock 4.2.6 software to predict the free binding energy (EFEB) of CPZ, CPZ photoproducts to several bacterial proteins, i.e., PBP3 MRSA, FtsA, PBP2a MRSA, PBP4, and FabL from *S. aureus*; PBP3 and PBP5 from *P. aeruginosa* and PBP3 from *E. coli* (Table 2).

Table 2. Lowest EFEB of CPZ and CPZ photoproducts in interaction with *S. aureus* six proteins, two *P. aeruginosa* proteins and one *E. coli* protein.

Lowest EFEB kcal/mol	CPZ	CPZ-SO	PZ	PZ-SO	HOPO	2HOPZSO	P1	P2
<i>S. aureus</i>								
PBP3 MRSA	-7.6	-6.0	-6.5	-5.6	-7.3	-6.7	-6.9	-7.2
FtsA	-8.7	-8.6	-7.1	-8.3	-7.5	-6.9	-7.7	-7.2
PBP2a MRSA (allosteric situs)	-7.6	-6.7	-6.3	-6.3	-6.8	-6.4	-7.2	-7.0
PBP2a MRSA (active situs)	-6.5	-6.0	-6.0	-5.7	-6.7	-6.8	-7.1	-5.9
PBP4	-6.70	-6.19	-5.67	-5.45	-6.23	-6.10	-6.25	-6.50
FabL	-8.30	-6.87	-7.16	-6.34	-7.74	-7.24	-7.74	-7.38
<i>P. aeruginosa</i>								
PBP3	-6.48	-4.55	-5.60	-3.70	-6.04	-5.77	-6.59	-6.63
PBP5	-6.79	-5.58	-5.45	-	-5.89	-5.61	-5.91	-5.80
<i>E. coli</i>								
PBP3	-6.77	-5.37	-5.88	-4.88	-5.96	-5.81	-6.06	-5.96

The Lowest EFEB was obtained for CPZ and *S. aureus* FtsA (-8.76 kcal/mol) and the highest EFEB was obtained for *P. aeruginosa* PBP3 and PZ-SO (Table 3). CPZ is interacting with FtsA in the active situs of the protein (Figure 2). In none of the simulated studies does a CPZ photoproduct exhibit a lower EFEB than CPZ. As for the biological activity on PBPs, CPZ and CPZ photoproducts present a low biological activity on *S. aureus* PBP2a and PBP3, and CPZ has no biological activity or almost no biological activity on *S. aureus* PBP4; *E. coli* PBP3; *P. aeruginosa* PBP3 and PBP5.

CPZ also presents a low EFEB in interaction with FabL (-8.30 kcal/mol) All CPZ photoproducts exhibit an EFEB similar to that of CPZ, as simulations have shown. As for the biological activity on PBPs, CPZ and CPZ photoproducts, they present no or a low biological activity on *S. aureus* PBP2a, PBP3, PBP4; *E. coli* PBP3; *P. aeruginosa* PBP3 and PBP5.

Table 3. MIC values for non-irradiated and laser irradiated solutions, against different microbial strains. MICs are expressed in $\mu\text{g/mL}$. NIR-CPZ = non-irradiated CPZ and IR-CPZ = irradiated CPZ.

Items	<i>S. aureus</i> ATCC 6538	MRSA1	MRSA2	<i>E. faecalis</i> ATCC 29212	<i>P. aeruginosa</i> ATCC 27853	<i>P. aeruginosa</i> clinic1	<i>P. aeruginosa</i> clinic2	<i>E. coli</i> ATCC 8739	<i>C. parapsilosis</i> ATCC 22019
NIR CPZ	100	100	100	50	>100	>100	>100	50	25
IR CPZ	12.5	12.5	6.25	6.26	100	100	100	25	6.25

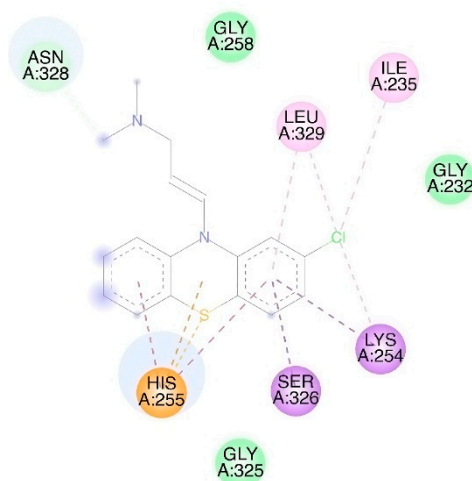


Figure 2. 2D visualization of interaction with the lowest EFEB between CPZ and FtsA (-8.7 kcal/mol) using Discovery studio visualizer [47]. Lys254 and His255 are AA in common with AA from the active site of FtsA.

3.2. pH Values

The pH values for non-irradiated CPZ and irradiated CPZ were 5.01 and 1.61, respectively. CPZ solutions were then mixed with culture medium. pH values were measured again, and determined as 7.11 pH for non-irradiated CPZ and 7.02 for irradiated CPZ.

3.3. Determination of Minimum Inhibitory Concentration (MIC)

Depending on the studied strain, non-irradiated and irradiated CPZ showed variable antimicrobial activity on the tested strains, as revealed by the different MIC values. Regarding the *E. faecalis* strains, the MIC value of the irradiated solution was much improved, from 50 $\mu\text{g/mL}$ to 6.25 $\mu\text{g/mL}$. In case of *S. aureus*, MIC values for non-irradiated solution were 100 $\mu\text{g/mL}$ for all three samples, while the MIC obtained for the irradiated compound ranged from 12.5 to 6.25 $\mu\text{g/mL}$.

The ability of CPZ to inhibit the Gram-negative bacteria growth was determined for *P. aeruginosa* and *E. coli*. The MIC for *P. aeruginosa* was established for three strains: a reference strains and two clinical isolates. The results indicated an MIC value of 100 $\mu\text{g/mL}$ for the irradiated CPZ, while for the non-irradiated CPZ the MIC was higher than the highest tested concentration. The Gram-negative bacteria have an outer membrane in addition to Gram-positive bacteria, and this may be the reason why they are more resistant to drug treatments. The antimicrobial effect of CPZ solutions is more visible for *E. coli* ATCC 8739 compared with *P. aeruginosa*; MIC values for *E. coli* ATCC are 50 $\mu\text{g/mL}$ for non-irradiated CPZ and 25 $\mu\text{g/mL}$ for irradiated CPZ.

In case of *Candida parapsilosis* ATCC strain, the MIC values were 25 $\mu\text{g/mL}$ for non-irradiated CPZ and 6.25 $\mu\text{g/mL}$ for laser exposed CPZ.

All the information is summarised in Table 3.

The stability of irradiated as well as non-irradiated compounds was also evaluated by determining the MIC after 4 months from the preparation of the solutions. The drug was stored at 4 °C in the dark.

For this experiment only three standard strains were tested, i.e.: *S. aureus* ATCC 6538, *P. aeruginosa* ATCC 27853 and *E. coli* ATCC 8739. As it can be seen in Figure 3, non-irradiated and irradiated CPZ solutions have retained their antimicrobial properties over time.

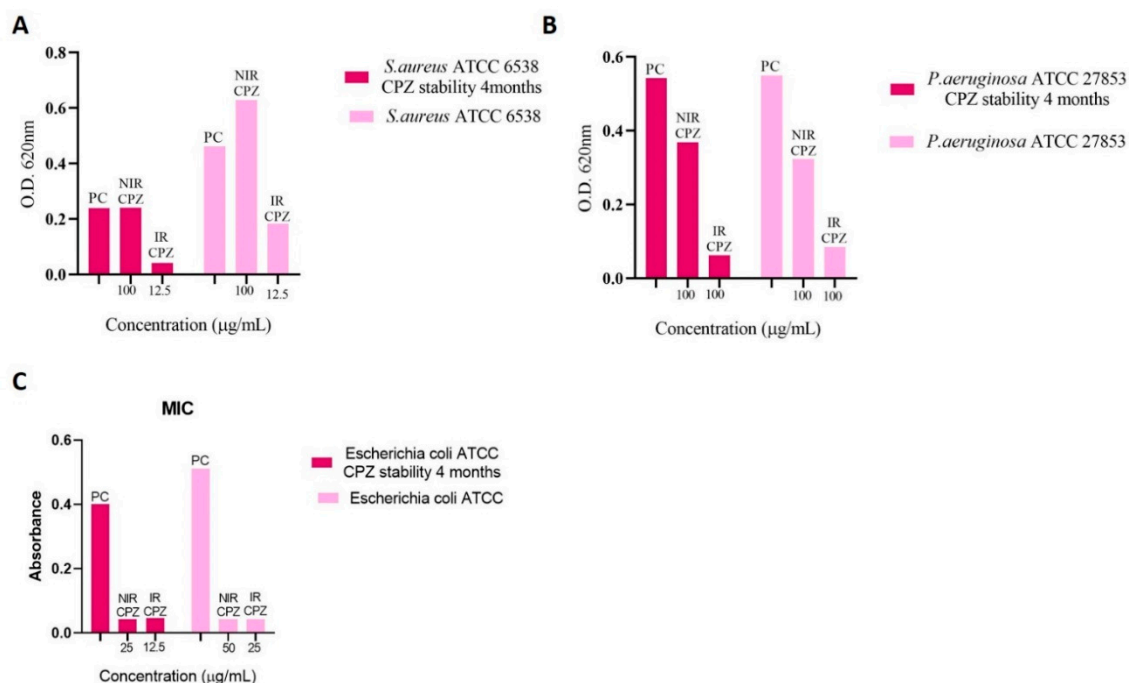


Figure 3. Stability of the antimicrobial activity of the tested compounds after 4 months from preparation of the non-irradiated and laser irradiated solutions. (A). *S. aureus* ATCC 6538, (B). *P. aeruginosa* ATCC 27853, and (C). *E. coli* ATCC 8739 Legend: PC = positive control, NIR-CPZ = non-irradiated CPZ and IR-CPZ = irradiated CPZ.

Using the same plates as for MIC assay, the biofilms formed on the microplate plastic walls were stained with crystal violet, and the MBEC values have been determined. For this experiment, the best anti-biofilm concentration was 6.25 µg/mL for irradiated CPZ (e.g., *E. faecalis* ATCC 29212 and/or MRSA2) and 100 µg/mL for non-irradiated CPZ (e.g., *S. aureus* ATCC 6538 and/or *P. aeruginosa* ATCC 27853).

3.4. Inhibition of Bacterial Adhesion on Cotton and Metal

In the case of *S. aureus* ATCC 6538, as seen in Figure 4B, cells adhesion to cotton patch immersed in irradiated CPZ was reduced drastically (from 1×10^7 CFU/mL to 30.3×10^4 CFU/mL). The non-irradiated drug has also inhibited the inhibit bacterial growth. Similar effects have been reported for *E. coli*. On the other hand, the cannula metal needle was difficult to impregnate with CPZ. Despite this fact, Figure 4A shows that anti-*S. aureus* ATCC 6538 activity increased even on this type of material. For the cannula, the number of *S. aureus* ATCC colonies was smaller than on cotton patch in all of samples. However, there is a difference between treatments: non-irradiated CPZ had a CFU/mL value of 27×10^3 and the irradiated one of 4.3×10^4 .

Furthermore, after we observed the effect against standard strains of the non-irradiated and laser exposed medicine, the same drug was used to demonstrate the efficiency across antibiotic resistant bacteria. Due to the large number of urinary tract infections, we examined the drug's effect on urinary catheters. The catheter segments were inoculated with two clinical MRSA and *P. aeruginosa* isolates. As shown in Figure 5B, the irradiation process improved the capacity of the antipsychotic drug to inhibit MRSA biofilm formation on the medical device compared to non-irradiated CPZ. Conversely, *P. aeruginosa* biofilm was not affected by the irradiation process of CPZ, since both

non-irradiated CPZ and irradiated CPZ lead to similar levels of microbial colonization on urinary catheters (Figure 5A).

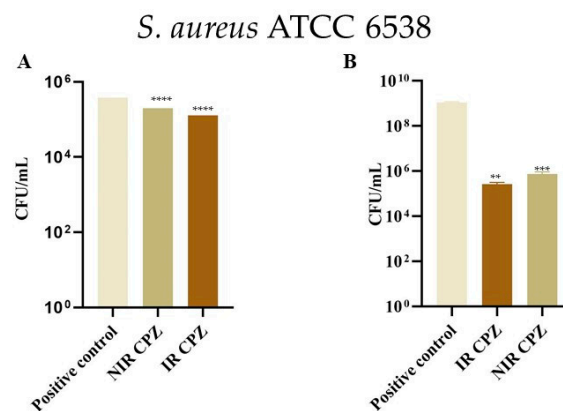


Figure 4. CFU/mL of *S. aureus* ATCC 6538 after 24 h on (A). cannula patch and (B). cotton treated before with non-irradiated and laser irradiated solutions. Legend: NIR-CPZ = non-irradiated CPZ and IR-CPZ = irradiated CPZ (data expressed as Mean \pm SEM, data points analysed by *t*-test, levels of statistical significance between the analysed groups: **** $p \leq 0.0001$, ** $p \leq 0.05$, *** $p \leq 0.001$). The positive control is represented by bacterial cultures alone.

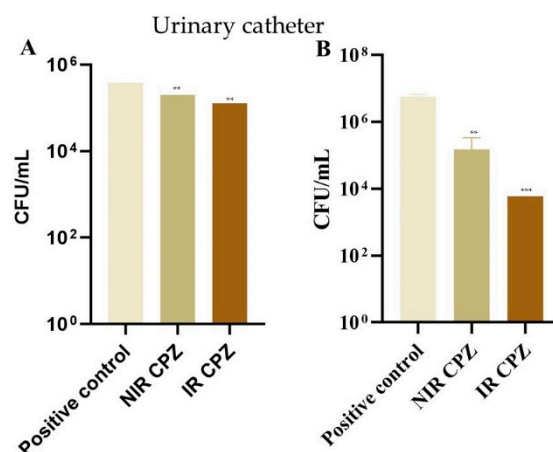


Figure 5. The values of CFU/mL for (A). *P. aeruginosa* clinic, (B). MRSA, attached on silicone urinary catheter, all catheter pieces were treated before with non-irradiated and irradiated CPZ solutions. Legend: NIR-CPZ = non-irradiated CPZ and IR-CPZ = irradiated CPZ (data expressed as Mean \pm SEM, data points analysed by *t*-test, levels of statistical significance between the analysed groups: ** $p \leq 0.05$, *** $p \leq 0.001$). The positive control is represented by bacterial cultures alone.

4. Discussion

Our study was focused on testing an antipsychotic drug (CPZ), in unirradiated and laser irradiated form, against various microorganisms of clinical importance. The reduced pH of laser exposed CPZ compared to non-irradiated CPZ can be explained by the photoionization process occurred during UV laser exposure of solutions. The possible pathways for the photodecomposition of CPZ were detailed by Alexandru et al. [23], reporting the formation of photoproducts like PZ through dechlorination, CPZ-SO, and PZ-SO via oxidation and/or hydrolysis, PZ-OH, PZ-OH-SO, and other three unidentified compounds.

Due to the highly hydrophobic ring and the hydrophilic side chain extension at N-10 position together with the substituent at C-2 position, phenothiazines act similarly to surfactants [51],

decreasing surface tension and improving wetting properties, as compared to water. It has been evidenced that irradiated CPZ exhibits even lower surface tension than non-irradiated CPZ. Regarding surface wettability, non-irradiated as well as irradiated CPZ had outstanding properties at 20 mg/mL concentration, as showed in Simon et al. [31].

The UV-Vis-NIR spectra of CPZ at 20 mg/mL analysed in Ref [31], show two absorbance peaks for unirradiated CPZ: at 254 nm and 306 nm (when diluted to 0.2 mg/mL). The interaction between 266 nm laser beam at 6.5 mJ and phenothiazine solution was studied for exposures from 1 min to 4 h; during irradiation a new shoulder was formed between 500 nm and 550 nm, and a new spectral band was located at 948 nm after 4 h of laser exposure. The appearance of these broad peaks in the Vis and NIR spectral range is due to the generation of photoproducts occurred during UV laser exposure of samples (i.e., free radicals' formation, such as chlorine atom, neutral promazinyl, hydroxyl, sulfur peroxy and cation radicals [23,28]). It has to be mentioned that the peak in the NIR region vanishes after 24 h following the irradiation process, suggesting that it belongs most probably to transient, short lifetime compounds, as presented in Refs. [28]. Therefore, the corresponding photoproducts are not anymore present in the solution at the time of the microbial assays.

Irradiated CPZ proved to have an antimicrobial effect both against susceptible and resistant bacteria, in planktonic and biofilm growth state. The mixture of photoproducts obtained after 4 h irradiation improves the bactericidal ability of the drug, as revealed by the decreased active concentrations.

Also, antipsychotic medicines may be used to protect medical devices against biofilm formation. We identified three possible causes of higher bacterial inhibitory activity of irradiated CPZ: (i) the main target of irradiated CPZ is an unstudied protein; (ii) CPZ generated photoproducts have a higher biological activity than non-irradiated CPZ. They may be responsible for the higher inhibitory activity of irradiated CPZ; (iii) the higher inhibitory activity of irradiated CPZ is given by the combined action of photoproducts on the biological target.

In a previous work we have tested the biological activity of CPZ-SO and PZ on several bacterial strains in comparison with CPZ and in all cases, we have obtained a lower MIC on CPZ than CPZ-SO and PZ. In another previous study, we proved that CPZ acts by targeting the efflux pumps [52,53]. Taking into consideration the similar MIC values obtained for different bacterial strains, we postulated that another essential well-conserved bacterial region is targeted by CPZ. We first thought at PBPs, but the results obtained were not too encouraging. Therefore, we tested FtsA and the FabL enzyme, which has an essential, but still unexplored role in the biosynthesis of fatty acids that may represent a new target. Results on both FtsA and FabL are encouraging, with CPZ presenting good EFEB. Regarding FtsA, the differences between EFEB of CPZ and CPZ-SO and PZ are small (Table 3). In the case of FabL, predicted results fit with the experimental ones [30], both CPZ-SO and PZ having higher EFEB than CPZ (Table 3). Taking all of the above into account, we consider that, most likely, the higher inhibitory action of irradiated CPZ is given by the combined action of the photoproducts on the biological target.

Our data are in accordance with similar studies performed by other research groups. CPZ was reported to harbor antimicrobial activity against a wide array of microorganisms such as *Salmonella enterica*, *Mycobacterium tuberculosis*, *S. aureus*, *P. aeruginosa*, *E. coli*, *Klebsiella pneumoniae*, and *Acinetobacter baumannii* [54,55]. A recent study by Sidrim et al. [56] showed that *E. coli*, *Proteus mirabilis* and *K. pneumoniae* biofilms grown on CPZ-impregnated catheters harbored significantly lower biofilm thickness and biomass and biomass compared to those of the growth control.

5. Conclusions

The increasing rates of antibiotic resistance and the urgent demand for novel therapeutic strategies lead to drug repurposing for fighting biofilm-associated infections. In line with this, chlorpromazine is not an antimicrobial drug, hence it does not act on the molecular targets of classic antibacterial agents; therefore, it may not affect the emergence of antibacterial resistance. Our research was focused on the efficiency of chlorpromazine, both non-irradiated and laser irradiated, against microorganisms

such as *S. aureus*, *E. faecalis*, *P. aeruginosa*, *E. coli*, and *C. parapsilosis*. We show that the antimicrobial activity was enhanced by laser exposure. Moreover, chlorpromazine-impregnated catheters reduced biofilm formation by *P. aeruginosa* and MRSA. We investigated the possible mechanisms underlying the improved antimicrobial activity of the irradiated chlorpromazine by molecular docking and showed that the higher inhibitory action of the irradiated compound was a result of the combined action of the photoproducts on the biological target. These preliminary results support the use of both irradiated and non-irradiated chlorpromazine as an adjuvant for preventing and treating infections related to medical devices (e.g., catheters, medicinal cotton).

Our results show that modifying the molecular structure of various drugs through laser radiation is a promising strategy to halt antibiotic resistance by repurposing current medicines for new therapeutic aims (anti-biofilm activity), thereby decreasing the costs and time for development of more efficient drugs.

Nevertheless, future studies are needed to better characterize and test *in vivo* this new therapeutic approach.

Author Contributions: S.N., data acquisition and processing, manuscript writing, G.G.P., methodology and data analysis, review and editing, A.-M.U., contribution to manuscript writing, molecular docking methods, Á.S., review and editing, contribution to conceptualization, M.L.P., manuscript editing, supervisor, experimental design, M.-C.C., manuscript editing, supervisor. All authors have read and agreed to the published version of the manuscript.

Funding: This work was supported by Romanian National Authority for Scientific Research and Innovation, CNCS/CCCDI-UEFISCDI, project PN- III-P1-1.1-PCCDI-2017-0728 and Nucleu Programme, ctr. No. 16N/08.02.2019.

Conflicts of Interest: The authors declare no conflict of interest.

References

1. Annual Report of the Chief Medical Officer Volume Two, 2011. Infections and the Rise of Antimicrobial Resistance. 2011; 154p. Available online: https://assets.publishing.service.gov.uk/government/uploads/system/uploads/attachment_data/file/138331/CMO_Annual_Report_Volume_2_2011.pdf (accessed on 7 June 2020).
2. McEwen, S.A.; Collignon, P.J. Antimicrobial Resistance: A One Health Perspective. In *Antimicrobial Resistance in Bacteria from Livestock and Companion Animals*; Schwarz, S., Cavaco, L.M., Shen, J., Eds.; American Society of Microbiology: Washington, DC, USA, 2018; pp. 521–547, ISBN 978-1-55581-979-8.
3. Sakko, M.; Tj, L. Microbiology of Root Canal Infections. *Prim. Dent. J.* **2016**, *5*, 84–89. [[CrossRef](#)] [[PubMed](#)]
4. Johani, K.; Abualsaud, D.; Costa, D.M.; Hu, H.; Whiteley, G.; Deva, A.; Vickery, K. Characterization of microbial community composition, antimicrobial resistance and biofilm on intensive care surfaces. *J. Infect. Public Health* **2018**, *11*, 418–424. [[CrossRef](#)] [[PubMed](#)]
5. Hall, C.W.; Mah, T.-F. Molecular mechanisms of biofilm-based antibiotic resistance and tolerance in pathogenic bacteria. *FEMS Microbiol. Rev.* **2017**, *41*, 276–301. [[CrossRef](#)] [[PubMed](#)]
6. Stewart, P.S.; Franklin, M.J. Physiological heterogeneity in biofilms. *Nat. Rev. Microbiol.* **2008**, *6*, 199–210. [[CrossRef](#)]
7. Welte, T. Nosocomial Infections—A Present and Future Challenge. *Dtsch. Arztebl. Int.* **2013**, *110*, 625–626. [[CrossRef](#)]
8. World Health Organization. *Report on the Burden of Endemic Health Care-Associated Infection Worldwide*; World Health Organization: Geneva, Switzerland, 2011.
9. Khan, H.A.; Baig, F.K.; Mehboob, R. Nosocomial infections: Epidemiology, prevention, control and surveillance. *Asian Pac. J. Trop. Biomed.* **2017**, *7*, 478–482. [[CrossRef](#)]
10. *Antimicrobial Resistance: Global Report on Surveillance*; World Health Organization: Geneva, Switzerland, 2014.
11. Emerson, C.B.; Eyzaguirre, L.M.; Albrecht, J.S.; Comer, A.C.; Harris, A.D.; Furuno, J.P. Healthcare-Associated Infection and Hospital Readmission. *Infect. Control Hosp. Epidemiol.* **2012**, *33*, 539–544. [[CrossRef](#)]
12. Safdar, N.; Maki, D.G. The Commonality of Risk Factors for Nosocomial Colonization and Infection with Antimicrobial-Resistant *Staphylococcus aureus*, *Enterococcus*, Gram-Negative Bacilli, *Clostridium difficile*, and *Candida*. *Ann. Intern. Med.* **2002**, *136*, 834–844. [[CrossRef](#)]
13. Roy, R.; Tiwari, M.; Donelli, G.; Tiwari, V. Strategies for combating bacterial biofilms: A focus on anti-biofilm agents and their mechanisms of action. *Virulence* **2018**, *9*, 522–554. [[CrossRef](#)]

14. Tamura, N.K.; Gasparetto, A.; Svidzinski, T.I.E. Evaluation of the Adherence of *Candida* Species to Urinary Catheters. *Mycopathologia* **2003**, *156*, 269–272. [[CrossRef](#)]
15. Davies, J. Inactivation of antibiotics and the dissemination of resistance genes. *Science* **1994**, *264*, 375–382. [[CrossRef](#)] [[PubMed](#)]
16. Pascu, M.L. (Ed.) *Laser Optofluidics in Fighting Multiple Drug Resistance*; Bentham Science Publishers: Sharjah, UAE, 2017; ISBN 978-1-68108-498-5.
17. van Duin, D.; Paterson, D.L. Multidrug-Resistant Bacteria in the Community. *Infect. Dis. Clin. N. Am.* **2016**, *30*, 377–390. [[CrossRef](#)] [[PubMed](#)]
18. USDA Agricultural Research Service; Allen, H.K. Alternatives to Antibiotics: Why and How. *NAM Perspect.* **2017**, *7*. [[CrossRef](#)]
19. Sudeshna, G.; Parimal, K. Multiple non-psychiatric effects of phenothiazines: A review. *Eur. J. Pharmacol.* **2010**, *648*, 6–14. [[CrossRef](#)]
20. Otręba, M.; Zdybel, M.; Pilawa, B.; Beberok, A.; Wrześniok, D.; Rok, J.; Buszman, E. EPR spectroscopy of chlorpromazine-induced free radical formation in normal human melanocytes. *Eur. Biophys. J.* **2015**, *44*, 359–365. [[CrossRef](#)]
21. MacAllister, S.L.; Young, C.; Guzdek, A.; Zhidkov, N.; O'Brien, P.J. Molecular cytotoxic mechanisms of chlorpromazine in isolated rat hepatocytes. *Can. J. Physiol. Pharmacol.* **2013**, *91*, 56–63. [[CrossRef](#)]
22. Pascu, M.L.; Danko, B.; Martins, A.; Jedlinszki, N.; Alexandru, T.; Nastasa, V.; Boni, M.; Militaru, A.; Andrei, I.R.; Staicu, A.; et al. Exposure of Chlorpromazine to 266 nm Laser Beam Generates New Species with Antibacterial Properties: Contributions to Development of a New Process for Drug Discovery. *PLoS ONE* **2013**, *8*, e55767. [[CrossRef](#)]
23. Alexandru, T.; Staicu, A.; Pascu, A.; Radu, E.; Stoicu, A.; Nastasa, V.; Dinache, A.; Boni, M.; Amaral, L.; Pascu, M.L. Characterization of mixtures of compounds produced in chlorpromazine aqueous solutions by ultraviolet laser irradiation: Their applications in antimicrobial assays. *J. Biomed. Opt.* **2014**, *20*, 051002. [[CrossRef](#)]
24. Drucker, A.M.; Rosen, C.F. Drug-Induced Photosensitivity: Culprit Drugs, Management and Prevention. *Drug Saf.* **2011**, *34*, 821–837. [[CrossRef](#)]
25. Vlad, I.M.; Nuta, D.C.; Chirita, C.; Caproiu, M.T.; Draghici, C.; Dumitrascu, F.; Bleotu, C.; Avram, S.; Udrea, A.M.; Missir, A.V.; et al. In Silico and In Vitro Experimental Studies of New Dibenz[b,e]oxepin-11(6H)one O-(arylcarbamoyl)-oximes Designed as Potential Antimicrobial Agents. *Molecules* **2020**, *25*, 321. [[CrossRef](#)]
26. Limban, C.; Dițu, L.M.; Măruțescu, L.; Missir, A.V.; Chifiriuc, M.C.; Căproiu, M.T.; Morusciag, L.; Chiriță, C.; Udrea, A.-M.; Nuță, D.C.; et al. Design, Synthesis and Biopharmacological Profile Evaluation of New 2-((4-Chlorophenoxy)methyl)-N-(Arylcarmothioyl)Benzamides with Broad Spectrum Antifungal Activity. *COC* **2019**, *23*, 1365–1377. [[CrossRef](#)]
27. Tozar, T.; Pascu, M.L. Time Stability of Laser Exposed Phenothiazines Aqueous Solutions in View of Antimicrobial Research. *Proc. Rom. Acad. Ser. A* **2018**, *19*, 537–544.
28. Andrei, I.R.; Tozar, T.; Dinache, A.; Boni, M.; Nastasa, V.; Pascu, M.L. Chlorpromazine transformation by exposure to ultraviolet laser beams in droplet and bulk. *Eur. J. Pharm. Sci.* **2016**, *81*, 27–35. [[CrossRef](#)]
29. Andrews, J.M. Determination of minimum inhibitory concentrations. *J. Antimicrob. Chemother.* **2001**, *48* (Suppl. 1), 5–16. [[CrossRef](#)] [[PubMed](#)]
30. Fisher, L.E.; Hook, A.L.; Ashraf, W.; Yousef, A.; Barrett, D.A.; Scurr, D.J.; Chen, X.; Smith, E.F.; Fay, M.; Parmenter, C.D.J.; et al. Biomaterial modification of urinary catheters with antimicrobials to give long-term broadspectrum antibiofilm activity. *J. Control. Release* **2015**, *202*, 57–64. [[CrossRef](#)] [[PubMed](#)]
31. Simon, A.; Alexandru, T.; Boni, M.; Damian, V.; Stoicu, A.; Dutschk, V.; Pascu, M.L. Interaction of solutions containing phenothiazines exposed to laser radiation with materials surfaces, in view of biomedical applications. *Int. J. Pharm.* **2014**, *475*, 270–281. [[CrossRef](#)] [[PubMed](#)]
32. Morán, M.C.; Tozar, T.; Simon, A.; Dinache, A.; Smarandache, A.; Andrei, I.R.; Boni, M.; Pascu, M.L.; Cirisano, F.; Ferrari, M. Toxicity study in blood and tumor cells of laser produced medicines for application in fabrics. *Colloids Surf. B Biointerfaces* **2016**, *137*, 91–103. [[CrossRef](#)]
33. Ananthkrishnan, N.; Rao, R.S.; Shivam, S. Bacterial adherence to cotton and silk sutures. *Natl. Med. J. India.* **1992**, *5*, 217–218.

34. Fage, C.D.; Lathouwers, T.; Vanmeert, M.; Gao, L.; Vrancken, K.; Lammens, E.; Weir, A.N.M.; Degroote, R.; Cuppens, H.; Kosol, S.; et al. The Kalimantacin Polyketide Antibiotics Inhibit Fatty Acid Biosynthesis in *Staphylococcus aureus* by Targeting the Enoyl-Acyl Carrier Protein Binding Site of FabI. *Angew. Chem. Int. Ed.* **2020**, *59*, 10549–10556. [[CrossRef](#)]
35. Fujita, J.; Maeda, Y.; Nagao, C.; Tsuchiya, Y.; Miyazaki, Y.; Hirose, M.; Mizohata, E.; Matsumoto, Y.; Inoue, T.; Mizuguchi, K.; et al. Crystal structure of FtsA from *Staphylococcus aureus*. *FEBS Lett.* **2014**, *588*, 1879–1885. [[CrossRef](#)]
36. Mahasenan, K.V.; Molina, R.; Bouley, R.; Batuecas, M.T.; Fisher, J.F.; Hermoso, J.A.; Chang, M.; Mobashery, S. Conformational Dynamics in Penicillin-Binding Protein 2a of Methicillin-Resistant *Staphylococcus aureus*, Allosteric Communication Network and Enablement of Catalysis. *J. Am. Chem. Soc.* **2017**, *139*, 2102–2110. [[CrossRef](#)] [[PubMed](#)]
37. Yoshida, H.; Kawai, F.; Obayashi, E.; Akashi, S.; Roper, D.I.; Tame, J.R.H.; Park, S.-Y. Crystal Structures of Penicillin-Binding Protein 3 (PBP3) from Methicillin-Resistant *Staphylococcus aureus* in the Apo and Cefotaxime-Bound Forms. *J. Mol. Biol.* **2012**, *423*, 351–364. [[CrossRef](#)] [[PubMed](#)]
38. Alexander, J.A.N.; Chatterjee, S.S.; Hamilton, S.M.; Eltis, L.D.; Chambers, H.F.; Strynadka, N.C.J. Structural and kinetic analyses of penicillin-binding protein 4 (PBP4)-mediated antibiotic resistance in *Staphylococcus aureus*. *J. Biol. Chem.* **2018**, *293*, 19854–19865. [[CrossRef](#)] [[PubMed](#)]
39. Sainsbury, S.; Bird, L.; Rao, V.; Shepherd, S.M.; Stuart, D.I.; Hunter, W.N.; Owens, R.J.; Ren, J. Crystal Structures of Penicillin-Binding Protein 3 from *Pseudomonas aeruginosa*: Comparison of Native and Antibiotic-Bound Forms. *J. Mol. Biol.* **2011**, *405*, 173–184. [[CrossRef](#)]
40. Smith, J.D.; Kumarasiri, M.; Zhang, W.; Heseck, D.; Lee, M.; Toth, M.; Vakulenko, S.; Fisher, J.F.; Mobashery, S.; Chen, Y. Structural Analysis of the Role of *Pseudomonas aeruginosa* Penicillin-Binding Protein 5 in β -Lactam Resistance. *Antimicrob. Agents Chemother.* **2013**, *57*, 3137–3146. [[CrossRef](#)]
41. Sauvage, E.; Derouaux, A.; Fraipont, C.; Joris, M.; Herman, R.; Rocaboy, M.; Schloesser, M.; Dumas, J.; Kerff, F.; Nguyen-Distèche, M.; et al. Crystal Structure of Penicillin-Binding Protein 3 (PBP3) from *Escherichia coli*. *PLoS ONE* **2014**, *9*, e98042. [[CrossRef](#)]
42. Harris, J.R.; Marles-Wright, J. (Eds.) *Macromolecular Protein Complexes II: Structure and Function; Subcellular Biochemistry*; Springer International Publishing: Cham, Switzerland, 2019; Volume 93, ISBN 978-3-030-28150-2.
43. Haenni, M.; Majcherczyk, P.A.; Barblan, J.-L.; Moreillon, P. Mutational Analysis of Class A and Class B Penicillin-Binding Proteins in *Streptococcus gordonii*. *Antimicrob. Agents Chemother.* **2006**, *50*, 4062–4069. [[CrossRef](#)]
44. Sauvage, E.; Kerff, F.; Terrak, M.; Ayala, J.A.; Charlier, P. The penicillin-binding proteins: Structure and role in peptidoglycan biosynthesis. *FEMS Microbiol. Rev.* **2008**, *32*, 234–258. [[CrossRef](#)]
45. Chen, W.; Zhang, Y.-M.; Davies, C. Penicillin-Binding Protein 3 Is Essential for Growth of *Pseudomonas aeruginosa*. *Antimicrob. Agents Chemother.* **2016**, *61*. [[CrossRef](#)]
46. Ropy, A.; Cabot, G.; Sánchez-Diener, I.; Aguilera, C.; Moya, B.; Ayala, J.A.; Oliver, A. Role of *Pseudomonas aeruginosa* Low-Molecular-Mass Penicillin-Binding Proteins in AmpC Expression, β -Lactam Resistance, and Peptidoglycan Structure. *Antimicrob. Agents Chemother.* **2015**, *59*, 3925–3934. [[CrossRef](#)]
47. BIOVIA. *Dassault Systèmes, [Discovery Studio Visualizer], [V20.1.0.19295]*; Dassault Systèmes: San Diego, CA, USA, 2019.
48. Morris, G.M.; Huey, R.; Lindstrom, W.; Sanner, M.F.; Belew, R.K.; Goodsell, D.S.; Olson, A.J. AutoDock4 and AutoDockTools4: Automated docking with selective receptor flexibility. *J. Comput. Chem.* **2009**, *30*, 2785–2791. [[CrossRef](#)] [[PubMed](#)]
49. Udrea, A.-M.; Avram, S.; Nistorescu, S.; Pascu, M.-L.; Romanitan, M.O. Laser irradiated phenothiazines: New potential treatment for COVID-19 explored by molecular docking. *J. Photochem. Photobiol. B Biol.* **2020**, *211*, 111997. [[CrossRef](#)] [[PubMed](#)]
50. Mitchell, M. *An Introduction to Genetic Algorithms*; Complex Adaptive Systems; MIT Press: Cambridge, MA, USA, 1996; ISBN 978-0-262-13316-6.
51. Kabir-ud-Din; Al-Ahmadi, M.D.A.; Naqvi, A.Z.; Akram, M. Micellar Properties of a Phenothiazine Drug in Presence of Additives. *Colloid J.* **2009**, *71*, 498–502. [[CrossRef](#)]

52. Tozar, T.; Nastasa, V.; Stoicu, A.; Chifiriuc, M.C.; Popa, M.; Kamerzan, C.; Pascu, M.L. In vitro antimicrobial efficacy of laser exposed chlorpromazine against Gram-positive bacteria in planktonic and biofilm growth state. *Microb. Pathog.* **2019**, *129*, 250–256. [[CrossRef](#)] [[PubMed](#)]
53. Grimsey, E.M.; Piddock, L.J.V. Do phenothiazines possess antimicrobial and efflux inhibitory properties? *FEMS Microbiol. Rev.* **2019**, fuz017. [[CrossRef](#)] [[PubMed](#)]
54. Bettencourt, M.V.; Bosne-David, S.; Amaral, L. Comparative in vitro activity of phenothiazines against multidrug-resistant *Mycobacterium tuberculosis*. *Int. J. Antimicrob. Agents* **2000**, *16*, 69–71. [[CrossRef](#)]
55. Nehme, H.; Saulnier, P.; Ramadan, A.A.; Cassisa, V.; Guillet, C.; Eveillard, M.; Umerska, A. Antibacterial activity of antipsychotic agents, their association with lipid nanocapsules and its impact on the properties of the nanocarriers and on antibacterial activity. *PLoS ONE* **2018**, *13*, e0189950. [[CrossRef](#)]
56. Sidrim, J.J.; Amando, B.R.; Gomes, F.I.; do Amaral, M.S.; de Sousa, P.C.; Ocadaque, C.J.; Brilhante, R.S.; A Cordeiro, R.D.; Rocha, M.F.; SCM Castelo-Branco, D.D. Chlorpromazine-impregnated catheters as a potential strategy to control biofilm-associated urinary tract infections. *Future Microbiol.* **2019**, *14*, 1023–1034. [[CrossRef](#)]

Publisher's Note: MDPI stays neutral with regard to jurisdictional claims in published maps and institutional affiliations.



© 2020 by the authors. Licensee MDPI, Basel, Switzerland. This article is an open access article distributed under the terms and conditions of the Creative Commons Attribution (CC BY) license (<http://creativecommons.org/licenses/by/4.0/>).